

Geophysical Research Letters



RESEARCH LETTER

10.1029/2020GL090921

Key Points:

- Distance to the magnetopause organizes compression-driven electromagnetic ion cyclotron (EMIC) wave observations better than L value
- EMIC waves in the magnetosphere are the most frequently observed close to the magnetopause model
- In this region EMIC waves are more frequent in the noon and dawn sectors than in the afternoon

Correspondence to:

B. Grison,
grison@ufa.cas.cz

Citation:

Grison, B., Santolík, O., Lukačević, J., & Usanova, M. E. (2021). Occurrence of EMIC waves in the magnetosphere according to their distance to the magnetopause. *Geophysical Research Letters*, 48, e2020GL090921. <https://doi.org/10.1029/2020GL090921>

Received 21 SEP 2020

Accepted 26 DEC 2020

Occurrence of EMIC Waves in the Magnetosphere According to Their Distance to the Magnetopause

B. Grison¹ , O. Santolík^{1,2} , J. Lukačević^{1,2} , and M. E. Usanova³ 

¹Department of Space Physics, Institute of Atmospheric Physics of the Czech Academy of Sciences, Prague, Czech Republic, ²Faculty of Mathematics and Physics, Charles University, Prague, Czech Republic, ³Laboratory for Atmospheric and Space Physics, University of Colorado Boulder, Boulder, CO, USA

Abstract Wave growth of electromagnetic ion cyclotron (EMIC) emissions observed in the outer magnetosphere is mainly controlled by compression events resulting from solar wind dynamic pressure pulses. During such events wave growth is expected to be maximum close to the magnetopause. In previous studies, distribution of EMIC waves was analyzed according to their distance from the Earth, which is inadequate for studying the magnetopause region. We map a data set of EMIC waves observed by Time History of Events and Macroscale Interactions during Substorms (THEMIS) spacecraft according to their distance from case-by-case modeled magnetopause. EMIC occurrence rate is found to be maximum within two Earth radii from the magnetopause and then it linearly decreases with an increasing distance, especially close to the local noon. Asymmetries between the morning and evening magnetic sectors are explained by asymmetries in the upstream conditions and by the presence of another EMIC population of a different origin.

Plain Language Summary The magnetopause is the boundary of the Earth's magnetosphere cavity in the heliosphere. When the magnetosphere is compressed by particles of solar origin (solar wind), the magnetopause is moving toward the Earth and specific waves, called electromagnetic ion cyclotron (EMIC), are expected to be strongly amplified just inside the magnetopause.

Several studies found that EMIC waves are more frequently observed at a larger distance from the Earth. The influence of the distance from magnetopause was thus never directly investigated because the magnetopause is not observed at a fixed distance from the Earth.

To address this problem, we use a magnetopause model whose position depends on solar wind properties. We then compute the distance from the magnetopause for a large data set of observed EMIC waves. Our results prove that EMIC waves in the outer magnetosphere are most frequently observed in the vicinity of the magnetopause, at distances less than two Earth radii. We also note and discuss a local time asymmetry in EMIC occurrence rates.

1. Introduction

Electromagnetic ion cyclotron (EMIC) emissions usually arise from hot proton temperature anisotropy (Kennel & Petschek, 1966). In the premidnight and dusk regions where the plasmopause boundary plays an important role (Tetrick et al., 2017), enhanced magnetospheric convection and ion injections consecutive to substorms are the main drivers of EMIC waves (Remya et al., 2020, and references therein). Temperature anisotropy can also result from a sudden increase in the magnetic field intensity through betatron acceleration. Terrestrial magnetosphere compression events, identified by sudden impulses in the Earth's magnetic field, are thus the main explanation of Pc1 waves (0.2–5 Hz, Jacobs et al. [1964]) observed frequently on the dayside from high-latitude ground stations (Hirasawa, 1981; Kangas et al., 1986; Olson & Lee, 1983).

Anderson et al. (1992) mapped EMIC waves observed in situ by AMPTE spacecraft in the magnetosphere between $L = 3.5$ and $L = 9$, where L is the McIllwain L -parameter. They found that EMIC waves are most frequently observed in the outer magnetosphere region, $L > 7$. According to ground-based observations amplifications of EMIC waves are correlated with modest magnetosphere compressions identified by in situ magnetic field intensifications (Anderson & Hamilton, 1993). These compression events result from increases of the solar wind dynamical pressure which are well correlated with EMIC wave observations (Usanova et al., 2012).

© 2021. The Authors.

This is an open access article under the terms of the [Creative Commons Attribution-NonCommercial-NoDerivs License](https://creativecommons.org/licenses/by-nc-nd/4.0/), which permits use and distribution in any medium, provided the original work is properly cited, the use is non-commercial and no modifications or adaptations are made.

All these studies note that the largest wave growth should be observed near the magnetopause. However, it is difficult to locate the continuously moving magnetopause, especially during magnetosphere compression events. Additionally, the inner magnetopause boundary is located at larger L on the flanks than in the subsolar region of the magnetosphere. Dependence on L or on radial distance is thus inadequate to study the EMIC occurrence in the vicinity of the magnetopause. Considering a magnetopause model, such as Shue et al. (1998) would be the adequate way to address this issue.

Occurrence rate of EMIC waves in the outer magnetosphere also varies with magnetic local time (MLT). In Anderson et al. (1992) the occurrence rate of the main population at large L is 10%–20% in the 11–15 MLT sector, and only 5% in the morning and evening sectors. Authors also note a monotonic increase with increasing L . Usanova et al. (2012) analyzed a database of EMIC observations by four of the Time History of Events and Macroscale Interactions during Substorms (THEMIS) spacecraft for $3 < L < 10$. The EMIC occurrence rate, always lower than 10%, is also found to peak at a large L with an increase in the 12–18 MLT sector. In the dawn sector the occurrence rate sharply increases in the largest L -bin (9.5–10). Allen et al. (2015) gathered 10 years of Cluster-4 spacecraft data to study EMIC properties as a function of the magnetic latitude in addition to L and MLT values. In L -MLT projection plane the maximum occurrence rate is again observed at large L ($L > 10$), in the afternoon sector followed by the dawn sector. These statistical studies all agree on the predominance of EMIC emissions at large L but they find some differences in the preferred MLT sectors. These differences can result from the inaccuracy of L -values to properly map the vicinity of the magnetopause.

Our goal is to map the EMIC emissions observed in situ according to their distance to the magnetopause and to the MLT. We can thus check if EMIC occurrence rate peaks close to the magnetopause and at which magnetic local time. In Section 2 we detail the magnetopause model (Shue et al., 1998) and the EMIC data set (Usanova et al., 2012) considered for our study. The distribution of EMIC emissions in the vicinity of the magnetopause is presented in Section 3. We discuss the validity of our results in Section 4. Conclusions are presented in Section 5.

2. Data Set and Methodology

Our study is based on the raw data set of EMIC events collected by Usanova et al. (2012) from the FGM instrument measurements (Auster et al., 2008) of the THEMIS mission (Angelopoulos, 2008). This data set contains about 28,000 EMIC events observed by the THEMIS A, C, D, and E spacecraft at radial distances (R^{sat}) smaller than $10 R_E$. Each event lasts 3 min and their identification between 0.1 and 2 Hz, 2 Hz being the FGM Nyquist frequency, relies on an automatic detection algorithm (Bortnik et al., 2007). This frequency range mainly relates in the outer magnetosphere with He^+ band. For more details, readers are referred to Usanova et al. (2012). Input for our analysis is the universal time (UT) of each 3-min event from the list of Usanova et al. (2012). We note t_{0i} the time of the i -th EMIC event.

The magnetopause location is found with the Shue et al. (1997, 1998) two dimensional model that gives the location in $(X; \sqrt{Y^2 + Z^2})$ half-plane, assuming an axial symmetry. ($X; Y; Z$) can be equally given in GSE or GSM coordinate systems. Model inputs are interplanetary magnetic field (IMF) B_z and solar wind dynamic pressure P_{dyn} . We extract B_z and P_{dyn} propagated to the bow-shock nose location, from 5-min resolution NASA/GSFC's OMNI data set (King & Papitashvili, 2005). We average B_z and P_{dyn} during 10 min starting from $t_{0i} - 20$ min. Time intervals $[t_{0i} - 20 \text{ min}; t_{0i} - 10 \text{ min}]$ are assumed to reflect the interplanetary conditions prior to the EMIC events, including propagation time of pressure pulses through the magnetosphere.

Figure 1 illustrates how we proceed considering an EMIC event of the original data set projected into $(X; \sqrt{Y^2 + Z^2})$ half-plane. The spacecraft location is marked with a triangle and the magnetopause is drawn in purple. The shortest distance from the two dimensional magnetopause is D_i^{2d} , found between the spacecraft position and point M_i^{2d} on the magnetopause. As the Shue et al. (1998) model is rotationally symmetric, the same shortest distance is also found in three dimensions. Since EMIC wave occurrence is mainly controlled by solar wind pressure pulses, the distance to magnetopause along the X-axis, D_i^X found between the spacecraft and point M_i^X on the magnetopause, makes also sense for this study. The selected EMIC event in

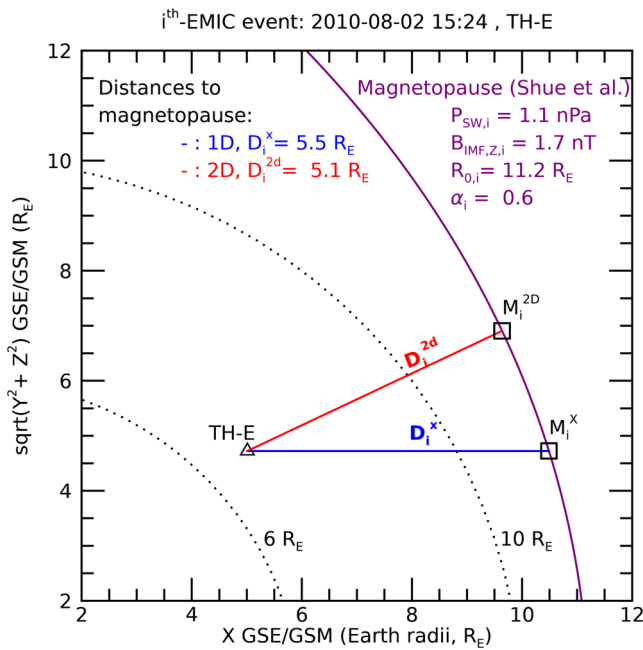


Figure 1. Illustrative case of electromagnetic ion cyclotron (EMIC) event (August 2, 2010 15:24:19, THEMIS-E) projected in the $(X; \sqrt{Y^2 + Z^2})$ GSE/GSM plane. Spacecraft location is marked by a triangle; magnetopause and related Shue et al. (1998) parameters are in purple. Two spacecraft-magnetopause distances are drawn in red (D^{2d}) and in blue (D^X). Black dotted curves mark equidistant location from the Earth (6 and 10 Earth radii).

to the magnetopause (D^{2d} in green and D^X in blue, upper abscissa). We choose opposed orientations of lower and upper abscissa to facilitate comparisons between R^{sat} , L , D^{2d} , and D^X . Roughly speaking regions closer to the Earth are on the left-hand side and regions closer to the magnetopause are on the right-hand side. We output the results in $1 R_E$ wide bins, as it is the order of the standard deviation of the magnetopause model.

We retrieve the previously known results that EMIC events are more numerous and more frequent with increasing distance from the Earth and increasing L values (black and red solid lines). Occurrence rates versus R^{sat} and versus L values are close to each other. By definition R^{sat} is always smaller than the corresponding L . The last L bin contains also some $L > 10$ values. The way we estimate the distance to the magnetopause has no influence on the wave event distribution (see green and blue lines). We now focus on D^{2d} , but our comments are also valid for D^X . The regular increase of EMIC counts with increasing distance to Earth also

results from the orbital motion of the spacecraft that dwell more time at larger radial distances. The occurrence rate of the EMIC events linearly increases when approaching the magnetopause up to $2 R_E$ (right panel, blue and green lines). It maximizes above 8% in the (1; 2] R_E bin. In association with a low number of EMIC events ($\approx 1,000$ events), the occurrence rate slightly decreases in the last bin (below 8%). This point is discussed in Section 4.2.

The original data set is reduced to avoid false detections: following Usanova et al. (2012) we consider only EMIC events that are detected in three or more consecutive intervals, i.e., only events lasting at least 9 min. We restrict our study to the dayside magnetosphere, i.e., $X > 0$. We consider only events whose positions are predicted inside the magnetosphere ($D^{2d} > 0$ which is equivalent to $D^X > 0$).

We perform the same analysis over all 3-min interval of spacecraft positions between May 2007 and December 2011 satisfying the criteria used for the EMIC events ($X_i^{sat} \geq 0$, $R_i^{sat} \leq 10 R_E$, and $D^{2d} \geq 0$). The occurrence rate of the EMIC events is obtained by dividing the number of EMIC events in each bin by the total number of cases. Table 1 summarizes the number of events obtained by application of these successive criteria. The data set contains 16,244 3-min EMIC events and 635,368 3-min measurement intervals. Overall EMIC occurrence rate is 2.6% in this data set.

3. Results: Influence of the Distance to Magnetopause

3.1. EMIC Occurrence Rate

Number and occurrence rates of EMIC events found between 8 and 16 MLT are presented in Figure 2. The number of EMIC events (left panel) and their occurrence rates (right panel) are plotted as a function of increasing distance from the Earth R^{sat} (in black, lower abscissa), increasing L (in red, lower abscissa), and decreasing distances to the magnetopause (D^{2d} in green and D^X in blue, upper abscissa). We choose opposed orientations of lower and upper abscissa to facilitate comparisons between R^{sat} , L , D^{2d} , and D^X . Roughly speaking regions closer to the Earth are on the left-hand side and regions closer to the magnetopause are on the right-hand side. We output the results in $1 R_E$ wide bins, as it is the order of the standard deviation of the magnetopause model.

The occurrence rate as a function of decreasing D^{2d} is larger than the occurrence as a function of increasing R^{sat} or L in all the bins. This figure proves that D^{2d} organizes better the EMIC events than R^{sat} or L in the outer magnetosphere and that the EMIC wave occurrence rate maximizes close to the magnetopause ($< 2 R_E$), and not simply at larger distances from Earth.

Table 1
Counts of 3-Min Events for EMIC Observations and for Spacecraft Location for Successive Selection Criteria

Counts	$R_i^{sat} \leq 10$	And ≥ 9 min	And $X_i^{sat} \geq 0$	And $D_i^{2d} \geq 0$
Measurement intervals	1,429,042	n/a	706,996	635,368
EMIC intervals	28,007	27,335	17,920	16,244

Note. $X_i^{sat} \geq 0$ events correspond to events observed in the dayside magnetosphere.

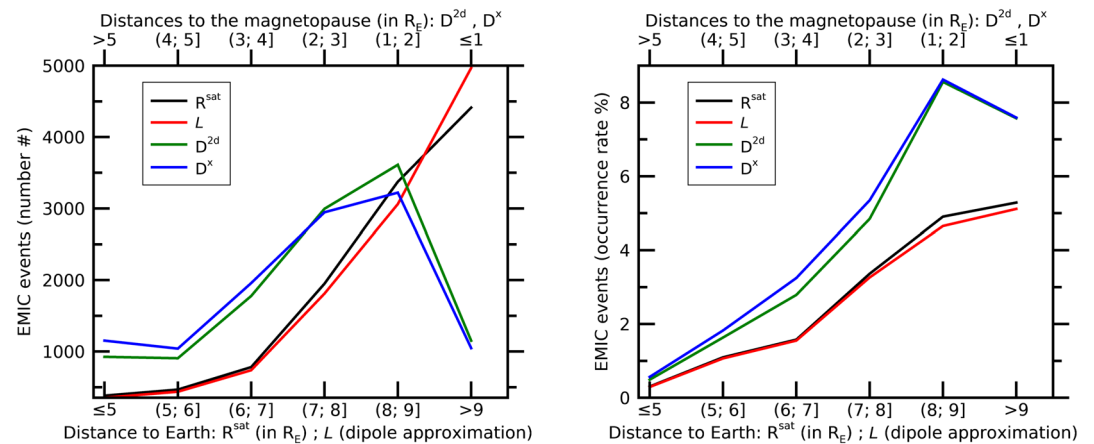


Figure 2. Number (left panel) and occurrence rate (right panel) of EMIC events observed up to 10 Earth radii (R_E), between 8 and 16 MLT, by the Time History of Events and Macroscale Interactions during Substorms (THEMIS) spacecraft. Results are presented as a function of L (in red), the distance to Earth R^{sat} (in black) or to the modeled magnetopause (absolute distance D^{2d} in green and distance toward the Sun D^x in blue). Upper and lower abscissa have opposite orientations to make comparisons easier.

3.2. Magnetic Local Time Dependence of the Occurrence Rate

The dependence on MLT of the EMIC waves distribution is investigated by comparing mapping obtained for D^{2d} and R^{sat} in Figure 3. As mentioned in previous section D^x and D^{2d} provide close results, R^{sat} and L too. We choose R^{sat} rather than L values because the R^{sat} data set is a bit larger when considering fixed bin width as there are events located at $L > 10$. Events predicted up to $1 R_E$ outside the magnetosphere are also included, with negative D^{2d} values.

During the considered periods, THEMIS dwelt a longer time at large R^{sat} , predominantly in the noon and afternoon sectors (top left panel of Figure 3). In the same data set, considering now D^{2d} , the spacecraft location for $\text{MLT} > 16$ h (in the evening sector) is found most of the time at a distance larger than $4 R_E$ from the magnetopause (bottom left panel). The same holds true for the morning sector with $\text{MLT} < 8$ h. On the other hand, for MLT between 8 and 16 h, the spacecraft was more often closer to the magnetopause, especially around the local noon. This results from the shape of the magnetosphere: as our data set is limited to $R^{\text{sat}} \leq 10 R_E$, spacecraft events observed close to the magnetopause in the morning and evening sectors are limited to infrequent highly compressed magnetosphere episodes. During these episodes the magnetosphere can either compress or relax. They should thus not be related to an artificially increased number of pressure-pulse related EMIC events as compression phases only are expected to be in favor of more EMIC wave observations. The influence of the absolute P_{dyn} values on the EMIC wave occurrence rate should also be investigated more in details.

The EMIC occurrence rate increases at large R^{sat} and it maximizes below 8% in the noon sector from 7 to 10 R_E (top right panel). EMIC events are more frequently observed in the dusk sector than in the dawn sector at all R^{sat} bins except for $R^{\text{sat}} > 9 R_E$, where EMIC wave occurrence rates are rather symmetrical around noon.

When considering D^{2d} dependence, bins where spacecraft dwelt less than 12 h (240 3-min events) are excluded from the occurrence rate calculations (white bins in the bottom right panel). This is the reason why occurrence rates in Figure 2 are calculated between 8 and 16 MLT. We remark that:

- Next to the magnetopause, in the magnetosphere ($0 < D^{2d} \leq 1 R_E$), EMIC waves are frequently observed between 12 and 13 MLT (occurrence rate larger than 13%) and are not common after 14 MLT
- In the noon MLT sector (11–14 MLT), EMIC waves occurrence rate is continuously decreasing with increasing distance to the magnetopause
- The region with the highest occurrence rates is the dawn sector (6–9 MLT) between 1 and 3 R_E to the magnetopause. Unfortunately, our data set did not sufficiently sample the closest bins to the magnetopause

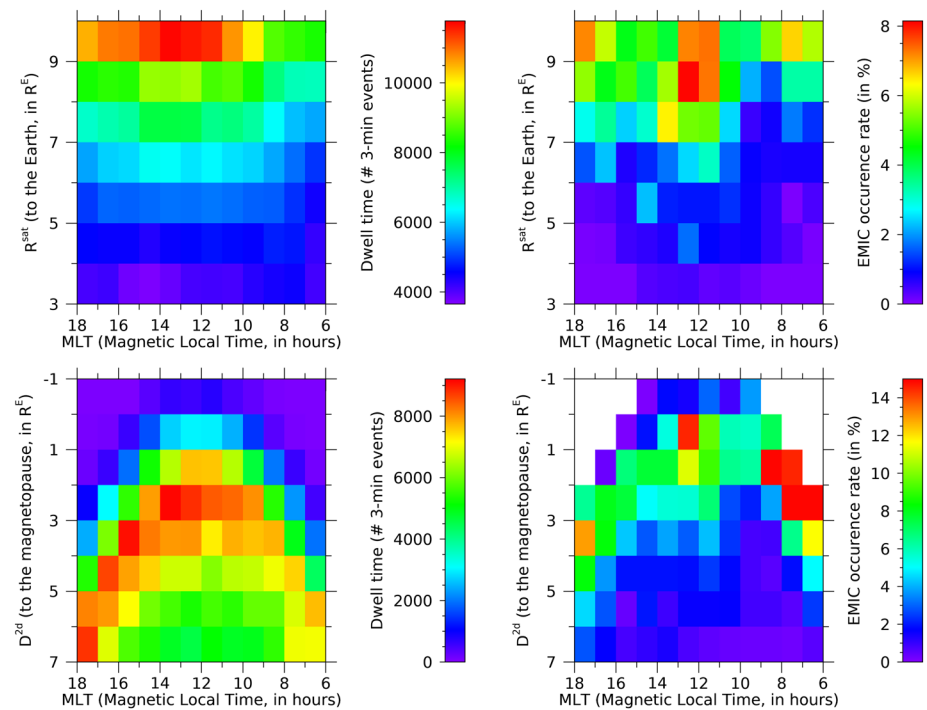


Figure 3. Dependence on MLT of EMIC emissions. Dwell time of the THEMIS spacecraft (left panels) and EMIC occurrence rate (right panels) are obtained according to distance to Earth R^{sat} (top panels) and modeled magnetopause (bottom panels). Occurrence rate values in the white bins are void due to a low dwell time value (less than 12 h). Note the different color scales. Events predicted outside the magnetosphere have negative D^{2d} values.

- When $D^{2d} > 3 R_E$, EMIC events are more frequent in all bins of the 16–18 MLT sector than in the mirroring bins of the morning sector. In 7 (of 8) bin pairs the occurrence rate differences between mirroring bins are larger than the uncorrelated error (9%) found in section 4.1, making this finding significant

Using D^{2d} rather than R^{sat} (or L) gives a different representation of the EMIC waves in the outer magnetosphere. EMIC waves are more frequent in the vicinity of the magnetopause than at large distance from the Earth (see the two different color scales in right panels of Figure 3). This is in agreement with a larger wave growth predicted close to the magnetopause during magnetosphere compression events. The predominance of EMIC waves in the morning MLT sector when $D^{2d} < 3 R_E$ suggests that the magnetosphere compression is more effective on the dawn side than on the dusk side of the magnetosphere as discussed in next section. Finally the occurrence rate at distances larger than $3 R_E$ from the magnetopause is maximum in the 16–18 MLT. These wave events might be connected with energetic ions arriving from the nightside MLT sectors.

4. Discussion

4.1. Investigation of Potential Biases

A potential bias stems from the automatic detection procedure of EMIC emissions which may give us a certain percentage of false detections. We checked results of the automatic detection of EMIC emissions by visual inspection of the spectrogram for one spacecraft (THEMIS-A, 5,597 3-min EMIC events). In approximately 90% of the automatic detections, EMIC emissions are clearly visible in the magnetosphere. In few cases (less than 1%) EMIC waves are both automatically and visually detected in the magnetosheath but close to the magnetopause. In the remaining intervals (9%) EMIC are not clearly visible. This can result from false detection of EMIC waves, but also from a false visual nondetection, when narrowband waves are hidden in a broadband structure, or when the signals are weak. We did not notice any preferred location for these possible false detections that could affect our study.

The main limitation of our study is therefore the exact determination of the magnetopause location at the observation times. Shue et al. (1998) model has a precision of about $1 R_E$. This precision can be worse during strong or sudden magnetosphere compression events, the magnetopause being always closer to the Earth than the predicted one (Staples et al., 2020). During such events the distance to the magnetopause is overestimated by the model: EMIC might be even closer to the magnetopause than reported in previous sections. The $1 R_E$ order of precision is confirmed by direct comparisons of magnetopause locations observed by THEMIS to model predictions (Němeček et al., 2016). Alternatively, we could estimate the distance to the magnetopause location considering the previous or next magnetopause crossings. However, the magnetopause still moves between the wave observation time and the next/previous crossing, and the precision of its position then would also depend on the time delay between the wave event time and the magnetopause crossing time. We therefore decided not to use this method as it would add a nonsystematic uncertainty with no real improvement. The distance to the magnetopause can be improved in the future with a better magnetopause model or a global picture of the magnetopause as expected from the future SMILE mission.

Limiting the observations to $10 R_E$ introduces a bias, as $10 R_E$ corresponds to the magnetopause subsolar point for $P_{\text{dyn}} = 2.4 \text{ nPa}$ (case $B_z = 0$ in Shue et al. [1998] model). Wave events observed during low P_{dyn} periods are seldom located close to the magnetopause in our data set. The influence on the occurrence rate is not clear as EMIC observations are related to a jump in P_{dyn} rather than to high P_{dyn} values and even modest magnetosphere compression events can be linked to EMIC emissions (Anderson & Hamilton, 1993). We checked that limiting the events with $P_{\text{dyn}} \geq 2.4 \text{ nPa}$ does not affect the overall EMIC wave distribution.

4.2. Influence of the Distance to Magnetopause

The wave growth increase following magnetosphere compression is expected to be the largest near the magnetopause (Anderson & Hamilton, 1993). In that respect it is thus surprising to note a plateau in the EMIC occurrence rate between $2 R_E$ and the magnetopause (Figure 2). This is true for most MLT sectors, excepted between 12 and 13 MLT (Figure 3). It can result from a low number of events in the (0; 1] bin (Figure 2) or from combined effect of the model precision and different wave activity between the magnetosphere and the magnetosheath. The inaccuracies of the magnetopause model can cause that an event can be predicted in the magnetosheath when actually located in the magnetosphere and vice-versa. This should not substantially affect the spacecraft position statistics: a comparable number of spacecraft positions are wrongly predicted in the magnetosphere or in the magnetosheath. This is not the case for the wave events, as the dominant broadband wave activity in the magnetosheath is excluded by the EMIC detection algorithm (Bortnik et al., 2007). Consequently, wave events observed close to the inner magnetosphere boundary but predicted outside are more numerous than the wave events observed in the magnetosheath but predicted close to the inner magnetosphere boundary. The occurrence found in the (0; 1] R_E range can be therefore considered as a lower estimate. We can only conclude that the wave growth is maximum within $2 R_E$ from the magnetopause. However the number of measurement intervals observed in the (-1; 0] bin (outside the magnetosphere) in Figure 3 is very small and it is still possible that the plateau in the occurrence rate in the immediate vicinity of the magnetopause is a real effect. Saturation of the compression effects on the wave growth or the propagation of the compression effects in the magnetosphere are two possible explanations that should be investigated in the future.

The dependence on MLT shows that EMIC emissions are more frequent on the morning side than on the dusk side close to the magnetopause. Dawn-dusk asymmetries are a widely discussed topic (see review by A. P. Walsh et al. [2014] and references therein). However, the overall influence and degree of translation of the upstream asymmetries on the magnetosphere is still an open question. At the magnetopause itself, Kelvin-Helmholtz instability takes place more often on the dawnside flank than on the duskside one (Nykyri, 2013). However, resulting kinetic Alfvén waves, also observed in [0.1; 5] Hz frequency range, should not increase the EMIC wave occurrence rate as they have a broadband spectrum (Grison et al., 2005). B. M. Walsh et al. (2012) noted in a THEMIS study covering almost the same time period as the present one that the proton density and bulk velocity in the magnetosheath are greater on the dawnside region ($16 \leq \text{MLT} \leq 18$) than on the duskside in agreement with the expected effect of magnetohydrodynamic Parker spiral. Such asymmetry can make the dawn MLT region more sensitive to pressure pulses in the solar wind.

Inside the magnetosphere, at larger distances from the magnetopause, the EMIC waves occurrence rate is the largest in the 16–18 MLT sector (Figure 3). As the EMIC waves are observed at large radial distances, plasma sheet ions drifting on open paths are more probably involved, rather than ring current ions drifting on closed paths (Anderson et al., 1992). Plasmaspheric plumes, often observed in this region and sometimes associated with large triggered EMIC emissions (Grison et al., 2018), can also play a role during a high P_{dyn} to explain the EMIC wave occurrence rate (Usanova et al., 2013).

The maximum occurrence rate is larger than the one observed in Usanova et al. (2012) with the same data set, showing that EMIC waves in the outer magnetosphere region are more dependent on the distance to the magnetopause than on the distance to Earth. It is worth to notice that we never find occurrence rate values as high as 20% which were reported by Anderson et al. (1992). The criterion of wave activity found during three or more consecutive 3-min intervals that we use in the present study is much more restrictive than the criterion of one or more peaks during a 5-min interval used by Anderson et al. (1992). Being more restrictive obviously leads to lower occurrence rates.

5. Conclusion

Mapping the distribution of EMIC waves according to L values or according to the radial distance from Earth R^{sat} provide similar results in the outer magnetosphere region (see Figure 2). This representation is not adapted for studying the role of the distance to magnetopause whose position varies in space and time, while the EMIC wave growth is expected to be maximum close to the magnetopause after magnetosphere compression events.

As the exact magnetopause position is unknown at the EMIC waves observation time, the distance to magnetopause used in this study is calculated from a modeled magnetopause (Shue et al., 1998) for each of the 16,244 EMIC events observed by the THEMIS spacecraft. The definition of the distance to the magnetopause, along one or two dimensions (D^x or D^{2d}) has no significant impact on the wave event distribution. We conclude that such mapping provides a more realistic distribution of EMIC wave occurrence rate in the outer magnetosphere, compared to mapping based on R^{sat} or L .

This mapping provides the experimental confirmation that occurrence rates of EMIC waves are maximum in the vicinity of the magnetopause, at distances lower than $2 R_E$ from the magnetopause. This EMIC population is obviously related to magnetosphere compression events. At larger distances, the EMIC occurrence rate linearly decreases with the increasing distance from the magnetopause. This is particularly true in the noon magnetic sector where the compression effects are expected to be the strongest.

EMIC waves are more often present in the vicinity of the magnetopause in the morning MLT sector than in the afternoon sector. The reason of this asymmetry comes probably from asymmetries in the proton density and bulk velocities observed in the magnetosheath. The exact importance of the magnetopause for EMIC wave at the flanks should be investigated with a data set containing EMIC observations at radial distances larger than $10 R_E$.

At distances larger than $3 R_E$, occurrence rates are larger in the evening sector than in the other sectors. That second EMIC population is possibly related to energetic ions coming from the nightside. The two EMIC populations are better disentangled when mapping according to D^{2d} than when mapping according to L or R^{sat} .

The occurrence rate is mostly constant in $[0-2] R_E$ range from the magnetopause. This would need further investigations with a larger data set of waves close to the magnetopause along with a better magnetopause location. Improving the precision of the magnetopause location can come from a more precise model and/or new observations of the future SMILE mission.

Data Availability Statement

The THEMIS/L2/FGM data set are accessible at <http://themis.ssl.berkeley.edu/data/themis/tha/l2/fgm> or via the repository <http://doi.org/10.17616/R37M05h>. The OMNI 5-min data set is accessible at https://spdf.gsfc.nasa.gov/pub/data/omni/high_res_omni/ or via the repository <http://doi.org/10.17616/R3TH0D>.

Acknowledgments

We acknowledge support of GACR Grant 18-05285S and of the Praemium Academiae Award. This project has received funding from the European Union's Horizon 2020 research and innovation programme under grant agreement No. 870452 (PAGER). We acknowledge use of NASA/GSFC's Space Physics Data Facility's ftp service and OMNI data. We acknowledge V. Angelopoulos for use of data from the THEMIS mission, and K. H. Glassmeier, U. Auster, and W. Baumjohann for the use of FGM data provided under the lead of the Technical University of Braunschweig and with financial support through the German Ministry for Economy and Technology and the German Center for Aviation and Space (DLR) under Contract 50 OC 0302.

References

- Allen, R. C., Zhang, J.-C., Kistler, L. M., Spence, H. E., Lin, R.-L., Klecker, B., et al. (2015). A statistical study of EMIC waves observed by Cluster: 1. Wave properties. *Journal of Geophysical Research: Space Physics*, *120*(7), 5574–5592. <https://doi.org/10.1002/2015JA021333>
- Anderson, B. J., Erlandson, R. E., & Zanetti, L. J. (1992). A statistical study of Pc 1–2 magnetic pulsations in the equatorial magnetosphere: 1. Equatorial occurrence distributions. *Journal of Geophysical Research*, *97*(A3), 3075–3101. <https://doi.org/10.1029/91JA02706>
- Anderson, B. J., & Hamilton, D. C. (1993). Electromagnetic ion cyclotron waves stimulated by modest magnetospheric compressions. *Journal of Geophysical Research*, *98*(A7), 11369–11382. <https://doi.org/10.1029/93JA00605>
- Angelopoulos, V. (2008). The THEMIS mission. *Space Science Reviews*, *141*(1), 5. <https://doi.org/10.1007/s11214-008-9336-1>
- Auster, H. U., Glassmeier, K. H., Magnes, W., Aydogar, O., Baumjohann, W., Constantinescu, D., et al. (2008). The THEMIS fluxgate magnetometer. *Space Science Reviews*, *141*(1), 235–264. <https://doi.org/10.1007/s11214-008-9365-9>
- Bortnik, J., Cutler, J. W., Dunson, C., & Bleier, T. E. (2007). An automatic wave detection algorithm applied to Pc1 pulsations. *Journal of Geophysical Research*, *112*, A04204. <https://doi.org/10.1029/2006JA011900>
- Grison, B., Hanzelka, M., Breuillard, H., Darrouzet, F., Santolik, O., Cornilleau-Wehrin, N., & Dandouras, I. (2018). Plasmaspheric plumes and EMIC rising tone emissions. *Journal of Geophysical Research: Space Physics*, *123*(11), 9443–9452. <https://doi.org/10.1029/2018JA025796>
- Grison, B., Sahraoui, F., Lavraud, B., Chust, T., Cornilleau-Wehrin, N., Rème, H., et al. (2005). Wave particle interactions in the high-altitude polar cusp: A Cluster case study. *Annales Geophysicae*, *23*(12), 3699–3713. <https://doi.org/10.5194/angeo-23-3699-2005>
- Hirasawa, T. (1981). Effects of magnetospheric compression and expansion on spectral structure of ULF emissions. [Special issue] *National Institute Polar Research Memoirs*, *18*, 127–151.
- Jacobs, J. A., Kato, Y., Matsushita, S., & Troitskaya, V. A. (1964). Classification of geomagnetic micropulsations. *Journal of Geophysical Research*, *69*(1), 180–181. <https://doi.org/10.1029/JZ069i001p00180>
- Kangas, J., Aikio, A., & Olson, J. V. (1986). Multistation correlation of ULF pulsation spectra associated with sudden impulses. *Planetary and Space Science*, *34*(6), 543–553. [https://doi.org/10.1016/0032-0633\(86\)90092-9](https://doi.org/10.1016/0032-0633(86)90092-9)
- Kennel, C. F., & Petschek, H. E. (1966). Limit on stably trapped particle fluxes. *Journal of Geophysical Research*, *71*(1), 1–28. <https://doi.org/10.1029/JZ071i001p00001>
- King, J. H., & Papitashvili, N. E. (2005). Solar wind spatial scales in and comparisons of hourly wind and ace plasma and magnetic field data. *Journal of Geophysical Research: Space Physics*, *110*, A02104. <https://doi.org/10.1029/2004JA010649>
- Němeček, Z., Šafránková, J., Lopez, R., Dušák, Š., Nouzák, L., Přeč, L., et al. (2016). Solar cycle variations of magnetopause locations. *Advances in Space Research*, *58*(2), 240–248. <https://doi.org/10.1016/j.asr.2015.10.012>
- Nykyri, K. (2013). Impact of MHD shock physics on magnetosheath asymmetry and Kelvin-Helmholtz instability. *Journal of Geophysical Research: Space Physics*, *118*(8), 5068–5081. <https://doi.org/10.1002/jgra.50499>
- Olson, J. V., & Lee, L. C. (1983). Pc1 wave generation by sudden impulses. *Planetary and Space Science*, *31*(3), 295–302. [https://doi.org/10.1016/0032-0633\(83\)90079-X](https://doi.org/10.1016/0032-0633(83)90079-X)
- Remya, B., Sibeck, D. G., Ruohoniemi, J. M., Kunduri, B., Halford, A. J., Reeves, G. D., & Reddy, R. V. (2020). Association between EMIC wave occurrence and enhanced convection periods during ion injections. *Geophysical Research Letters*, *47*(3), e2019GL085676. <https://doi.org/10.1029/2019GL085676>
- Shue, J.-H., Chao, J. K., Fu, H. C., Russell, C. T., Song, P., Khurana, K. K., & Singer, H. J. (1997). A new functional form to study the solar wind control of the magnetopause size and shape. *Journal of Geophysical Research*, *102*(A5), 9497–9511. <https://doi.org/10.1029/97JA00196>
- Shue, J.-H., Song, P., Russell, C. T., Steinberg, J. T., Chao, J. K., Zastenker, G., et al. (1998). Magnetopause location under extreme solar wind conditions. *Journal of Geophysical Research*, *103*(A8), 17691–17700. <https://doi.org/10.1029/98JA01103>
- Staples, F. A., Rae, I. J., Forsyth, C., Smith, A. R. A., Murphy, K. R., Raymer, K. M., et al. (2020). Do statistical models capture the dynamics of the magnetopause during sudden magnetospheric compressions? *Journal of Geophysical Research: Space Physics*, *125*(4), e27289. <https://doi.org/10.1029/2019JA027289>
- Tetrick, S. S., Engebretson, M. J., Posch, J. L., Olson, C. N., Smith, C. W., Denton, R. E., et al. (2017). Location of intense electromagnetic ion cyclotron (EMIC) wave events relative to the plasmopause: Van Allen Probes observations. *Journal of Geophysical Research: Space Physics*, *122*(4), 4064–4088. <https://doi.org/10.1002/2016JA023392>
- Usanova, M. E., Darrouzet, F., Mann, I. R., & Bortnik, J. (2013). Statistical analysis of EMIC waves in plasmaspheric plumes from Cluster observations. *Journal of Geophysical Research: Space Physics*, *118*(8), 4946–4951. <https://doi.org/10.1002/jgra.50464>
- Usanova, M. E., Mann, I. R., Bortnik, J., Shao, L., & Angelopoulos, V. (2012). THEMIS observations of electromagnetic ion cyclotron wave occurrence: Dependence on AE, SYMH, and solar wind dynamic pressure. *Journal of Geophysical Research: Space Physics*, *117*, A10218. <https://doi.org/10.1029/2012JA018049>
- Walsh, A. P., Haaland, S., Forsyth, C., Keesee, A. M., Kissinger, J., Li, K., et al. (2014). Dawn-dusk asymmetries in the coupled solar wind-magnetosphere-ionosphere system: A review. *Annales Geophysicae*, *32*(7), 705–737. <https://doi.org/10.5194/angeo-32-705-2014>
- Walsh, B. M., Sibeck, D. G., Wang, Y., & Fairfield, D. H. (2012). Dawn-dusk asymmetries in the earth's magnetosheath. *Journal of Geophysical Research: Space Physics*, *117*(A12). <https://doi.org/10.1029/2012JA018240>